Solid-state n.m.r. studies of crystalline phases in gel-spun ultrahigh molecular weight polyethylene

D. L. Tzou, K. Schmidt-Rohr and H. W. Spiess*
Max-Planck-Institut für Polymerforschung, Postfach 3148, D-55021 Mainz, Germany
(Received 18 November 1993; revised 5 April 1994)

Gel-spun ultrahigh molecular weight polyethylene (UHMWPE) was examined by advanced solid-state ^{13}C n.m.r. techniques to extract detailed information on the morphology and nature of the crystalline phases. Two partially overlapping resonances separated by 1.5 ppm in the ^{13}C magic angle spinning n.m.r. spectrum have been assigned to monoclinic and orthorhombic crystalline phases. To analyse better the small amount of monoclinic phase, a ^{13}C chemical shift filter was employed to suppress partially the dominant orthorhombic signal. The monoclinic phase exhibits a slightly smaller chemical shielding anisotropy of 27 ppm with chemical shift principal tensor values of 50, 36.5 and 16 ppm as compared to a shielding anisotropy of 30 ppm and principal tensor values of 50, 35.5 and 13 ppm for the orthorhombic phase. Additionally, a minor fraction of interface was detected arising from heterogeneous molecular packing. Both crystalline phases reveal an extremely high degree of order, with $\langle p_2 \rangle$ around 0.94. Whereas the conformations of the chains in the non-crystalline regions of both gel-spun and melt-spun polyethylene are alike, the mobility of the former is largely reduced. The morphology of UHMWPE is compared with that of melt-spun polyethylene.

(Keywords: gel-spun polyethylene; ^{13}C n.m.r.; monoclinic phase)

INTRODUCTION

High performance gel-spun ultrahigh molecular weight polyethylene (UHMWPE)[1-5] has attracted much scientific interest in the last decade concerning its superior mechanical properties[6-14] and unique molecular structure[15-17]. The modulus of UHMWPE is in the region of 2000 cN dtex^{-1}†, which is at least two orders of magnitude above that of melt-spun polyethylene. Likewise, its tensile strength is about 15 times greater than that of normal melt-spun polyethylene[18]. The gel-spinning process has also been applied to other polymers, for example polypropylene, which show enormous improvements in molecular orientation[19]. To date, gel spinning represents the most successful method for converting polyethylene from a lamellar morphology to a fibrillar extended chain morphology[6,15,20-22]. It is generally agreed that gel-spun polyethylene fibres consist of macrofibres containing microfibrils of extended chains. Each of these chains exhibits a high degree of orientational order along the fibril axis, and in turn each of the fibrils along the fibre axis[15-17]. Investigations of the morphology which indicate this structure have been performed by means of small-angle X-ray scattering (SAXS)[23], wide-angle X-ray diffraction (WAXD)[24], differential scanning calorimetry (d.s.c.)[25,26], Raman spectroscopy[27] and solid-state n.m.r.[28-33].

Two crystalline phases are contained in gel-spun polyethylene, namely the well-known orthorhombic phase and a relatively small fraction of monoclinic phase[24,34]. Either one of them consists of molecular chains in an all-*trans* conformation. In the monoclinic phase, the planes formed by these zigzag chains are all aligned parallel, while in the orthorhombic phase these planes make up a perpendicular ('fish bone') mosaic pattern. A detailed characterization of these phases has been reported by VanderHart and Khoury[30]. A solid–solid phase transition converting the monoclinic into the orthorhombic phase at elevated temperatures below the melting point has been reported by several investigators[34,35]. In an alternative interpretation of the X-ray diffraction patterns, it was recently suggested that the crystalline structure can be described in terms of a defect model including perfect and imperfect segments[26]. A detailed characterization of the crystalline phases by n.m.r. has been lacking until now, owing to the difficulties of resolving overlapping ^{13}C resonances. Here we report the results of applying advanced solid-state n.m.r. techniques that quantify sample morphology and orientational order for the crystalline phases and non-crystalline regions in considerably greater detail.

EXPERIMENTAL

The experimental studies were carried out on samples of a commercially available gel-spun UHMWPE (Allied

* To whom correspondence should be addressed
† The 'unit' dtex is a measure of the linear density of fibres and corresponds to the mass in grams of 10000 m of fibres

0032-3861/94/22/4728-06

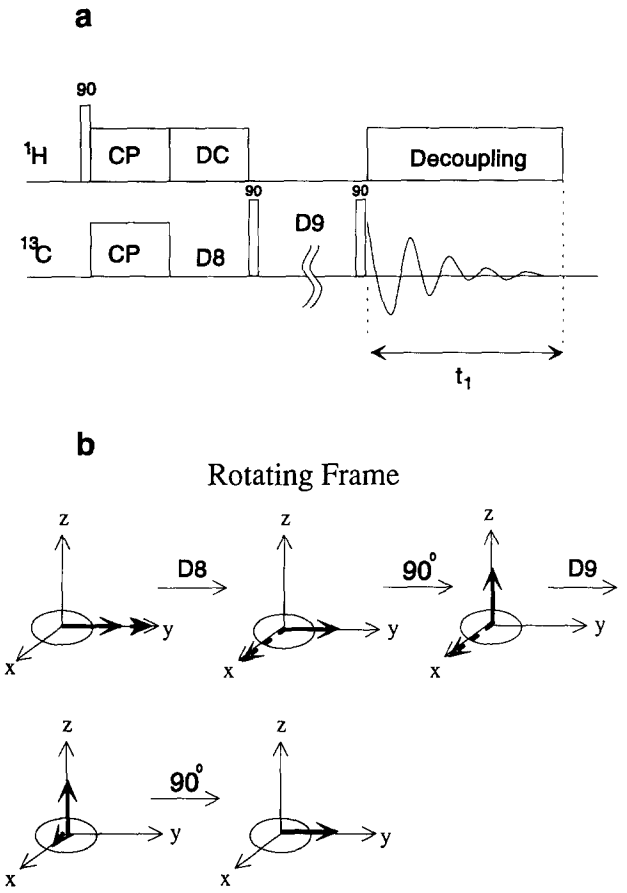

Figure 1 ^{13}C chemical shift filter technique: (a) pulse sequence; (b) illustration of the action of the chemical shift filter on two magnetization vectors in the rotating frame. DC denotes the SELDOM pulse sequence[37]; the delays D8 and D9 are explained in the text

Signal Spectra 1000 fibre, $M_w > 10^6\,g\,mol^{-1}$). Its non-crystalline fraction determined by X-ray measurements amounts to approximately 20%. In addition, a normal molecular weight melt-spun polyethylene (PE) was used as a reference. The mechanical properties of these samples have been reported elsewhere[18]. All the measurements were performed on a Bruker MSL300 spectrometer at a ^{1}H frequency of 300.13 MHz and a ^{13}C frequency of 75.47 MHz using a double-bearing Bruker magic angle spinning (m.a.s.) probe and 7 mm zirconium oxide rotors at ambient temperature. The 90° pulse width for the ^{1}H and ^{13}C pulses was 4 μs. The ^{13}C and ^{1}H wide line spectra detected by two-dimensional wide line separation (WISE) spectroscopy[36] were acquired with 64 t_1 increments of 5 μs with a 300 μs cross-polarization (c.p.) contact time. Incrementing the proton evolution time t_1 leads to a modulated ^{13}C signal, and subsequent two-dimensional Fourier transformation yields a spectrum with dipolar-broadened proton lines resolved in ω_2 by the carbon m.a.s. spectrum. Two-dimensional techniques including rotor-synchronized m.a.s. and exchange methods were employed, incorporating a ^{13}C chemical shift filter (SELDOM[37]) to suppress the dominant orthorhombic signal. As a requirement of the chemical shift filter pulse sequence the small downfield monoclinic peak was precisely set on resonance. The pulse sequence is given in *Figure 1a*. *Figure 1b* shows that after cross-polarization the magnetization vectors corresponding to the orthorhombic and monoclinic peaks precess away from each other in the rotating frame x–y plane because of the difference in chemical shift. After a time delay of D8 = 2050 μs, the magnetization vectors of the monoclinic and orthorhombic phases are 90° out of phase. This time delay must be equal to an m.a.s. rotor period (or a multiple of it), so the sample rotation frequency was chosen as 488 Hz. The desired monoclinic magnetization was stored along the z axis by flipping it back with a 90° pulse, while the orthorhombic magnetization was left in the x–y plane to dephase under ^{1}H dipolar couplings for a time period of D9 = 1 ms. The free induction decay (FID) was then acquired after a 90° readout pulse.

The chemical shift filter was combined with two-dimensional exchange and rotor synchronization methods mainly to suppress the orthorhombic intensity described above. Details of the two-dimensional exchange[38] and two-dimensional rotor synchronization[39] techniques have been reported elsewhere. Modified pulse sequences for these two techniques are given in *Figure 2*. In the two-dimensional exchange experiments, 40 FIDs were accumulated corresponding to a t_1 increment of 1600 μs with a mixing time of 1 s. In the rotor synchronization experiments FIDs were acquired separately for 16 starting rotor positions (see *Figure 2b*). Also in the rotor synchronization experiments, the filaments were aligned at 90° with respect to the rotor axis to achieve a better sample-filling factor. Consequently, no sideband intensity could be detected on odd-numbered slices[40].

RESULTS AND DISCUSSION

Shielding tensors of orthorhombic and monoclinic phases

The one-dimensional c.p./m.a.s. spectrum of gel-spun UHMWPE fibre is shown in *Figure 3a*. It can be seen

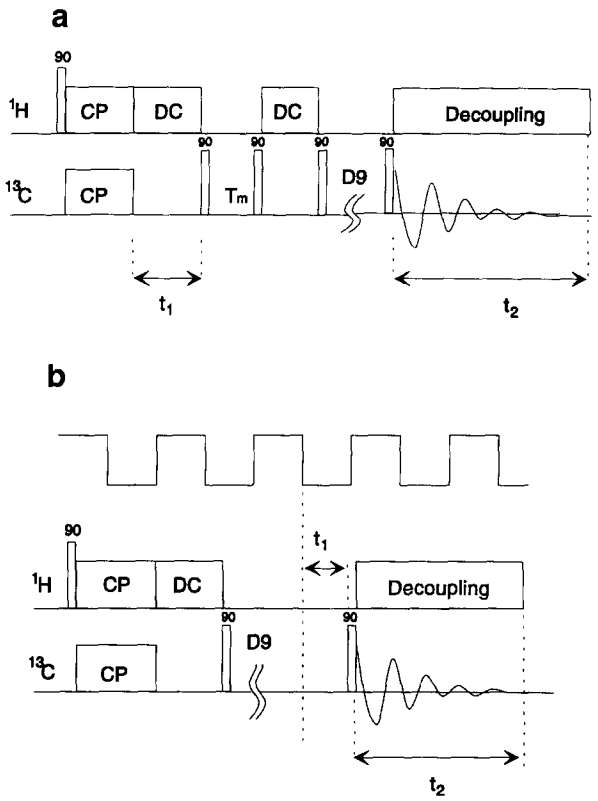

Figure 2 Two-dimensional n.m.r. experiments employed in this work: (a) pulse sequence with the chemical shift filter in the preparation period; (b) rotor-synchronized m.a.s. technique combined with chemical shift filter. See also *Figure 1*

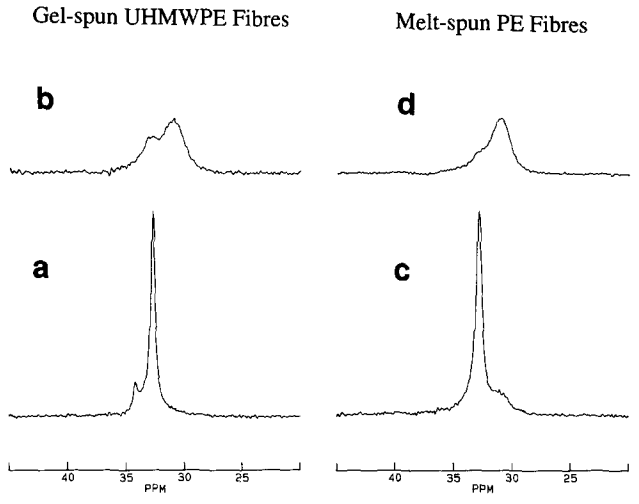

Figure 3 (a) ^{13}C c.p./m.a.s. spectrum for UHMWPE with a contact time of 1 ms. (b) ^{13}C single-pulse detection of the mobile component with a repetition time of 500 ms. The spectra in (c) and (d) were obtained from the same experiments as in (a) and (b), respectively, for normal molecular weight melt-spun PE. The peak intensities were scaled to equal peak heights between (b) and (d)

that a small peak appears at 1.5 ppm downfield of the dominant orthorhombic signal at 32.8 ppm (referenced to the upfield peak of adamantane at 29.5 ppm). This peak was assigned to the monoclinic phase in the UHMWPE sheet[30]. For convenience, the two phases are denoted as C1 (monoclinic) and C2 (orthorhombic) for the rest of the discussion. The two phases differ in their molecular packings, as described earlier.

In order to analyse the molecular structures in finer detail, the chemical shift filter technique described above was applied to scale the C2 intensity down to a level comparable to the C1 intensity, The result is shown in *Figure 4*. In addition to an isotropic shift difference between the two resonances of 1.5 ppm, two sideband envelopes with slightly different intensities can be seen. This suggests that the two crystalline structures differ slightly in their chemical shift anisotropies. The tensor elements for the C1 and C2 signals determined by Herzfeld and Berger's sideband analysis[41] are given in *Table 1*. The shielding anisotropy for the C1 phase is 2.5 ppm lower than that for the C2 phase, and one of the principal axes σ_{33}, which is aligned along the chain, is shifted by 3 ppm downfield in the C1 phase (see *Table 1*). This shows that the environments of the CH_2 groups are not identical. However, it is not obvious what the structural differences are, because presently the correlation between the chemical shielding effect and the molecular structure and packing is not sufficiently understood. Nevertheless, the chemical shift can be related to the structure by comparison with a model system. Thus, a similar examination was performed on the crystalline n-alkane eicosane, which has the same molecular packing as the monoclinic C1 phase[42]. Agreement between the chemical shift tensors of C1 and eicosane is found (see *Table 1*). This observation shows that the macrostructural packings in the crystallites can be detected in terms of both isotropic and anisotropic chemical shifts.

Orientational order

The chemical shift filter method was also combined with two-dimensional rotor-synchronized m.a.s.[39] and the two-dimensional exchange technique[43] to examine the crystalline phases. The rotor-synchronized m.a.s. experiment has been proven successful in characterizing molecular order in a number of polymer systems[39,44,45]. Applying the technique to gel-spun UHMWPE, indications were reported that the C1 phase was less oriented than the C2 phase[46]. However, uncertainties in the order parameters might have arisen from the limited spectral resolution and the absence of sufficiently intense higher order orientational sidebands in the C1 signal. In this study, we combined the chemical shift filter with two-dimensional rotor-synchronized m.a.s. to obtain a higher resolution for the crystallite resonances. The resulting spectrum is shown in *Figure 5a*. The orientational dimension (sidebands labelled M) is plotted vertically. It exhibits only even-numbered M slices because the sample was prepared such that the fibres were aligned perpendicular to the rotor axis[40]. Both phases clearly show similar sideband intensities along the orientational (M) dimension from $M=0$ to $M=\pm 4$. Similarity in the degrees of molecular order is indicated by the orientational sideband patterns, which result from molecular order via phase and amplitude modulation of the m.a.s. sidebands. Two order parameter sets, $\langle p_2 \rangle$ to $\langle p_8 \rangle$ with uncertainties of ± 0.05 (see *Table 2*), were obtained from a quantitative

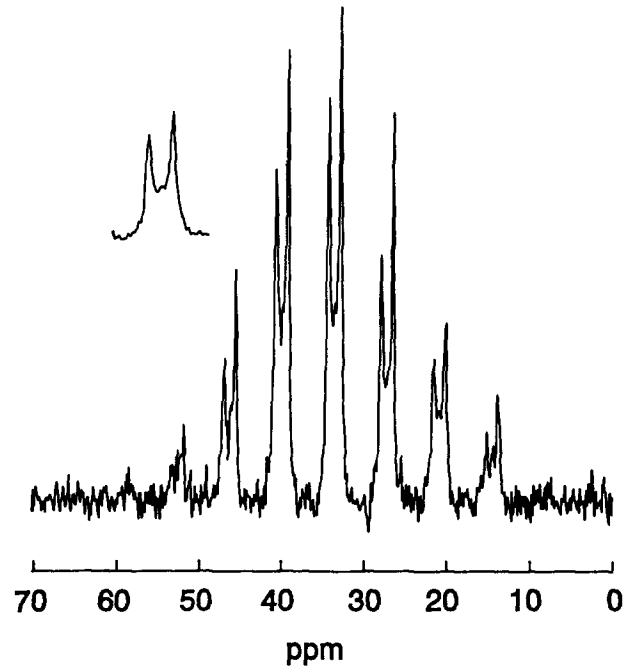

Figure 4 ^{13}C c.p./m.a.s. chemical shift filter spectrum at 488 Hz. The inset shows an expansion of the isotropic peak revealing an interface between C1 and C2 resonances (see text)

Table 1 Chemical shift tensor principal values[a] for gel-spun UHMWPE fibres

	σ_{11}	σ_{22}	σ_{33}	σ_{iso}	$\Delta\sigma^d$
C1 (monoclinic)[b]	50.1	36.5	16.0	34.2	−27.3
C2 (orthorhombic)[b]	50.1	35.3	13.0	32.8	−29.7
Eicosane (triclinic)[b]	50.4	36.8	15.7	34.3	−27.9
Eicosane (triclinic)[c]	49.1	37.1	16.1	34.1	−27.0

[a] In parts per million (ppm) referenced to the upfield peak of adamantane at 29.5 ppm
[b] Error limits are ±1.0 ppm
[c] Chemical shift tensor principal values determined by VanderHart[42]
[d] Shielding anisotropy $\Delta\sigma=\sigma_{33}-\frac{1}{2}(\sigma_{11}+\sigma_{22})$

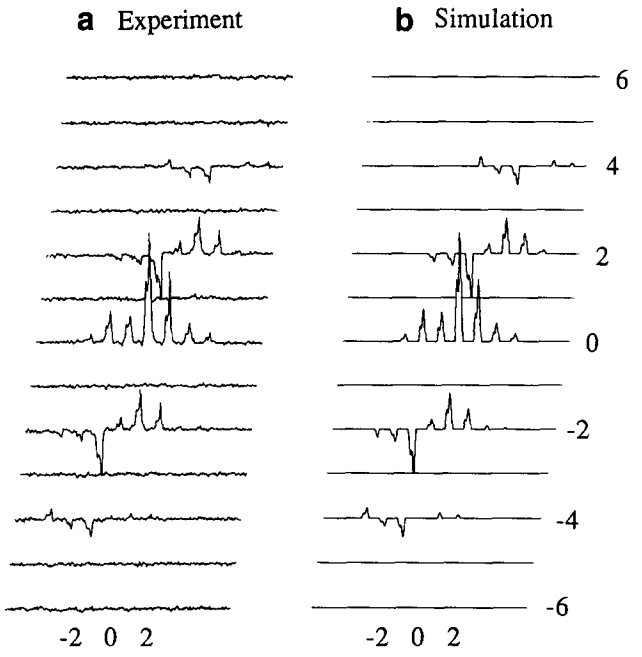

Figure 5 (a) Two-dimensional rotor synchronization chemical shift filter spectrum at a spinning speed of 488 Hz. Sixteen slices were acquired with 800 scans. The fibres were aligned perpendicular to the rotor axis. For this orientation only even-numbered sideband slices are observed. (b) Simulated spectrum calculated from the order parameters listed in *Table 2*

Table 2 Order parameters for gel-spun UHMWPE fibres

	C1	C2
$\langle P_2 \rangle$	0.93	0.96
$\langle P_4 \rangle$	0.80	0.82
$\langle P_6 \rangle$	0.78	0.80
$\langle P_8 \rangle$	0.61	0.62
$\langle P_{10} \rangle$		0.22

analysis of the sideband intensities. They reveal an extremely high degree of order for both the C1 and C2 phases. If the two phases were perfect and imperfect segments in the crystallites, respectively, as suggested by the defect model, they should exhibit distinctly different degrees of molecular orientation.

Detection of crystalline phases and the interface

Some information about the size of the C1 and C2 crystallites can be obtained from ^{13}C T_1 measurements[47]. The two phases exhibit rather different relaxation behaviour, with ^{13}C T_1 values of approximately 500 s and 1500 s for the C1 and C2 peaks, respectively[46]. This shows that on a time-scale of 1000 s, the ^{13}C magnetization in the two phases is not equilibrated by ^{13}C spin diffusion[48], indicating that the two phases are separated on a scale of nanometres.

In the chemical shift filtered spectrum in *Figure 4*, significant intensity is observed between the maxima of the two crystalline signals. In order to find out whether this comes from homogeneous line broadening of the two peaks or from different segments, we performed a two-dimensional exchange experiment with a short mixing time, where the linewidth perpendicular to the diagonal is determined solely by homogeneous line broadening and the linewidth along the diagonal is determined by both inhomogeneous and homogeneous line broadening[38,49]. To eliminate the peak overlap problem, again the chemical shift filter was implemented in the preparation period of the two-dimensional exchange experiment. The two-dimensional pattern plotted in *Figure 6* shows much larger linewidths along the diagonal, which proves that most of the line broadening is inhomogeneous. In particular, the ridge appearing between the C1 and C2 signals shows that a distribution of macromolecular environments exists, which strongly suggests the presence of an interface. As indicated in the contour plot, the inhomogeneous linewidth for C1 is slightly broader than that for C2. However, this inhomogeneous line broadening that arises from molecular packing does not indicate a lower orientational order in the C1 phase (see *Table 2*).

The signal for the non-crystalline phase, though not directly apparent in the cross-polarization spectra of *Figures 3a* and *4*, can be detected if a ^{13}C single-pulse excitation with a repetition time of 500 ms is utilized. The spectrum is exhibited in *Figure 3b* and can be compared with the corresponding signal from normal melt-spun PE shown in *Figure 3d*; the maximum peak intensities are scaled to equal heights. Although the UHMWPE fibres contain far fewer mobile domains than normal melt-spun PE, the line shapes of the non-crystalline peaks are essentially the same. Since the isotropic ^{13}C chemical shift depends on the chain conformation, this comparison implies that the conformational statistics in the non-crystalline regions are similar in the two samples.

In order to study the mobility of the segments in the non-crystalline phases, two-dimensional wide line separation (WISE) experiments were performed[36]. They provide separate ^1H wide line spectra by detecting proton magnetization in the first dimension via amplitude modulation of the ^{13}C magnetization, which provides a highly resolved ^{13}C m.a.s. spectrum in the second dimension. Thus, sample mobility information for the different structures can be obtained from the spectrum. In *Figure 7*, for both melt-spun PE (*Figure 7a*) and gel-spun UHMWPE (*Figure 7b*), the broad ^1H lines from the crystalline regions indicate rigid structures that arise from crystal packing. In contrast, the narrow ^1H line at

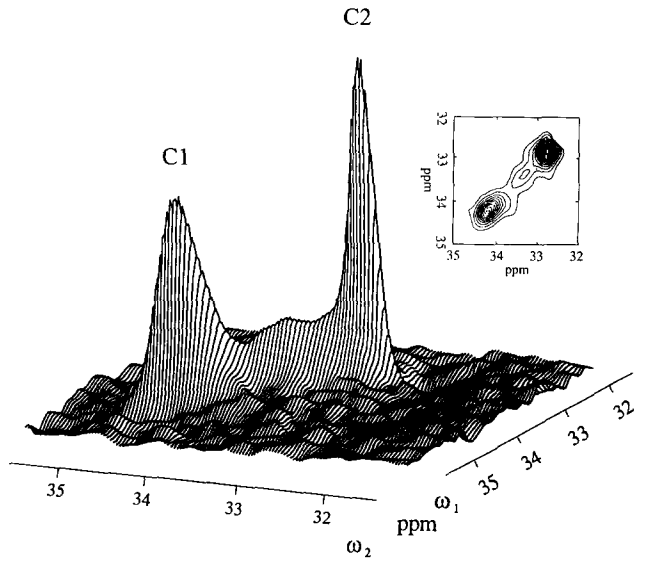

Figure 6 ^{13}C two-dimensional exchange spectrum after applying the ^{13}C chemical shift filter. In the upper right corner a contour plot is displayed

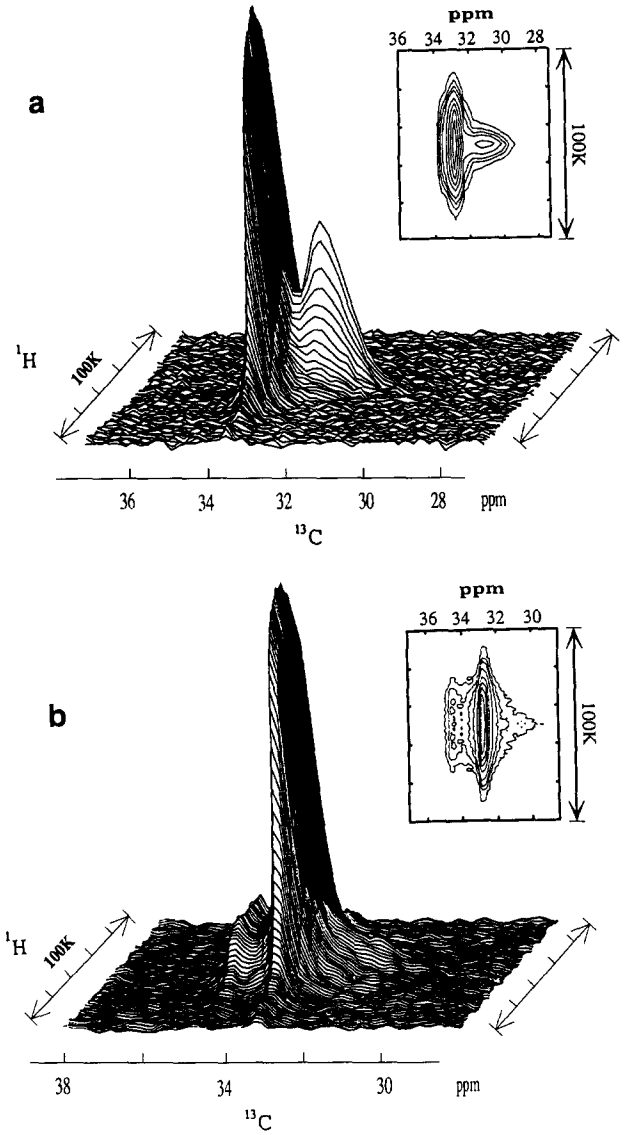

Figure 7 Two-dimensional WISE spectra: (a) normal melt-spun PE fibres; (b) gel-spun UHMWPE fibres. The insets show contour plots

the ^{13}C resonance of the non-crystalline region of normal PE, as seen in *Figure 7a*, indicates high segmental mobility. In the WISE spectrum of gel-spun UHMWPE (*Figure 7b*), the non-crystalline regions exhibit a significantly increased ^1H linewidth, and consequently considerably restricted mobility, compared to the non-crystalline regions of the normal PE sample. It is thus interesting to note that in spite of the similarity in line shapes (conformations) and T_1 relaxations (high frequency mobilities), in gel-spun UHMWPE the amplitudes of the kilohertz motions in the non-crystalline regions are much more restricted than in normal melt-spun PE.

Phase structure

Combining all these findings, we therefore propose a model for the phase structure in gel-spun UHMWPE that consists of four domains: 75% orthorhombic (C2), 15% monoclinic (C1) and 5% interfacial crystalline material, as well as about 5% non-crystalline material with some, though restricted, molecular motions. The relative fractions are estimates based on all the experiments described above and further checked by simulating the c.p./m.a.s. spectrum as a superposition of four lines at the respective isotropic chemical shifts and widths of 35 Hz for the crystalline and interfacial regions and 120 Hz for the non-crystalline regions. A schematic representation of the model is depicted in *Figure 8*. Note that representative chains in the respective regions are shown, not chains adjacent to each other.

In fact, our model of the chain packing in gel-spun PE is also consistent with recent Raman spectroscopic investigations[50], which detected a bimodal stress distribution in the crystalline regions upon deformation. This was attributed to high load bearing chains in regions adjacent to and low load bearing chains in regions remote from the defect structures. The fraction of high load bearing chains (40%) by far exceeds the fraction of taut-tie molecules or intercrystalline bridges which could be present in the 15% non-crystalline material of that sample. However, a different conclusion has been drawn from a combination of X-ray scattering and Raman spectroscopy[51].

The chain alignments in the orthorhombic and monoclinic domains are alike. The conformational disorder in

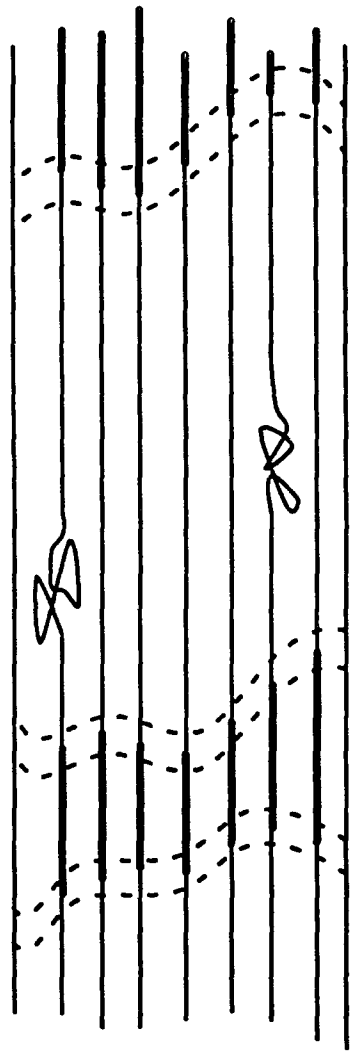

Figure 8 Macrostructural model for gel-spun UHMWPE fibres. Four different domains are included. The thin lines represent the C2 phase (orthorhombic), the bold lines show the C1 phase (monoclinic) and the areas between crystalline domains enclosed by dotted lines are interfacial regions. Additionally, the entangled curves indicate non-crystalline segments. Note that representative chains in the respective regions are shown, not chains adjacent to each other

the non-crystalline regions of gel-spun UHMWPE is as high as in the amorphous regions of melt-spun PE; however, large amplitude motions in the former are largely restricted, presumably because of the limited extent of these regions. Thus, the detailed characterization of the different domains provided by advanced solid-state n.m.r. techniques should help to relate better the macroscopic behaviour to the molecular parameters.

ACKNOWLEDGEMENTS

We would like to thank Dr R. Lewis for checking the manuscript and Dr S. Curran for helpful discussions during the early stages of this work. The gel-spun UHMWPE samples and financial support from Allied Signal Inc. are gratefully acknowledged. D. L. T. thanks the Max-Planck-Society for the provision of a stipend.

REFERENCES

1 Clifferri, A. and Ward, I. M. 'Ultrahigh Modulus Polymers', Applied Science, London, 1979, p. 1
2 Wu, W. and Black, W. B. *J. Polym. Eng. Sci.* 1979, **19**, 1163
3 Southern, J. H. and Porter, R. S. *J. Appl. Polym. Sci.* 1970, **14**, 2305
4 Zachariades, A. E. and Kanamoto, T. *J. Polym. Eng. Sci.* 1986, **26**, 658
5 Rotzinger, B. P., Chanzy, H. D. and Smith, P. *Polymer* 1989, **30**, 1814
6 Kavesh, S. and Prevorsek, D. C. *US Pat. 4413110*, 1983
7 Marichin, V. A., Mjasnikova, L. P., Zenke, D., Hirteand, R. and Weigel, P. *Polym. Bull.* 1984, **12**, 287
8 Torfs, J. C. M. and Pennings, A. J. *J. Appl. Polym. Sci.* 1987, **26**, 303
9 Hoogsteen, W., Kormelink, H., Eshuis, G., ten Brinke, G. and Pennings, A. J. *J. Mater. Sci.* 1988, **23**, 3459
10 Hoogsteen, W., Van der Hooft, R. J., Postema, A. R., ten Brinke, G. and Pennings, A. J. *J. Mater. Sci.* 1988, **23**, 3467
11 Smook, J. and Pennings, A. J. *J. Appl. Polym. Sci.* 1982, **27**, 2209
12 Smook, J. and Pennings, A. J. *J. Mater. Sci.* 1984, **19**, 31
13 Smook, J., Flinterman, M. and Pennings, A. J. *Polym. Bull.* 1980, **2**, 775
14 Smith, P., Lemstra, P. J., Kalb, B. and Pennings, A. J. *Polym. Bull.* 1979, **1**, 733
15 Van Hutten, P. F., Koning, C. E. and Pennings, A. J. *J. Mater. Sci.* 1985, **20**, 1556
16 Juska, T. and Harrison, I. R. *J. Mater. Sci.* 1982, **22**, 766
17 Pennings, A. J. in 'Proc. Int. Conf. on Crystal Growth' (Ed. H. S. Peiser), Pergamon Press, New York, 1967, p. 389
18 Tzou, D. L., Huang, T.-h., Saraf, A. W., Desai, P. and Abhiraman, A. S. *ACS PMSE Prepr.* 1991, **64**, 375
19 Cannon, C. G. *Polymer* 1982, **23**, 1123
20 Pennings, A. J., Smooks, J., de Boer, J., Gogolewski, S. and van Hutton, P. F. *Pure Appl. Chem.* 1983, **55**, 777
21 Barham, P. J. and Keller, A. *J. Mater. Sci.* 1985, **20**, 2281
22 Barham, P. J. *Polymer* 1982, **23**, 1112
23 Furuhata, K., Yokokawa, T., Seoul, C. and Miyasaka, K. *J. Polym. Sci., Polym. Phys. Edn* 1986, **24**, 59
24 Ottani, S., Wager, B. E. and Porter, R. S. *Polym. Commun.* 1990, **31**, 370
25 Tervoort-Engelen, Y. M. T. and Lemstra, P. J. *Polym. Commun.* 1991, **32**, 343
26 Saraf, A. W., Desai, P. and Abhiraman, A. S. *J. Appl. Polym. Sci., Polym. Symp.* 1991, **47**, 67
27 Wang, L. H., Porter, R. S., Stidham, H. D. and Hsu, S. L. *Macromolecules* 1991, **24**, 5535
28 Earl, W. L. and VanderHart, D. L. *Macromolecules* 1979, **12**, 762
29 Jarrett, W. L., Porter, R. S. and Mathias, L. J. *Polym. Prepr.* 1990, **31**, 647
30 VanderHart, D. L. and Khoury, F. *Polymer* 1984, **25**, 1589
31 Takenaka, K., Yamanobe, T., Komoto, T., Ando, I. and Sato, H. *Solid State Commun.* 1987, **61**, 563
32 Axelson, D. E., Mandelkern, L., Poplian, R. and Mathieu, P. *J. Polym. Sci., Polym. Phys. Edn* 1983, **21**, 2319
33 Kitamura, R., Horrii, F. and Murayama, K. *Macromolecules* 1986, **19**, 636
34 Takahashi, Y. and Ishida, T. *J. Polym. Sci., Polym. Phys. Edn* 1988, **26**, 2267
35 Seto, T., Hara, T. and Tanaka, K. *Jpn. J. Appl. Phys.* 1968, **37**, 31
36 Schmidt-Rohr, K., Clauss, J. and Spiess, H. W. *Macromolecules* 1992, **25**, 3273
37 Tekely, P., Brondeau, J., Elbayed, K., Retournard, A. and Canet, D. *J. Magn. Reson.* 1988, **80**, 509
38 Szeverenyi, N. M., Sullivan, M. J. and Maciel, G. E. *J. Magn. Reson.* 1982, **47**, 462
39 Harbison, G. S., Vogt, V.-D. and Spiess, H. W. *J. Chem. Phys.* 1986, **86**, 597
40 Munowitz, M. G. and Griffin, R. G. *J. Chem. Phys.* 1982, **76**, 2848
41 Herzfeld, J. and Berger, A. E. *J. Chem. Phys.* 1980, **73**, 6021
42 VanderHart, D. L. *J. Magn. Reson.* 1981, **44**, 117
43 Schmidt-Rohr, K. and Spiess, H. W. *Macromolecules* 1991, **24**, 5288
44 Harbison, G. S. and Spiess, H. W. *Chem. Phys. Lett.* 1986, **124**, 128
45 Blümich, B., Böffel, C., Harbison, G. S., Yang, Y. and Spiess, H. W. *Ber. Bunsenges. Phys. Chem.* 1987, **91**, 1100
46 Tzou, D. L., Huang, T.-h., Desai, P. and Abhiraman, A. S. *J. Polym. Sci., Polym. Phys. Edn* 1993, **31**, 1005
47 Torchia, D. A. *J. Magn. Reson.* 1978, **30**, 613
48 VanderHart, D. L. *J. Magn. Reson.* 1987, **72**, 13
49 Szeverenyi, N. M., Bax, A. and Maciel, G. E. *J. Am. Chem. Soc.* 1983, **105**, 2579
50 Wong, W. F. and Young, R. J. *J. Mater. Sci.* 1994, **24**, 520
51 Moonen, J. A. H. M., Roovers, W. A. C., Meier, R. J. and Kip, B. J. *J. Polym. Sci., Polym. Phys. Edn* 1992, **30**, 361